Divergent spatiotemporal integration of whole-field visual motion in medaka and zebrafish

Authors

Yasuko Isoe[1*], Yasmine Fatima Mabene[2], Marie-Abèle Bind[2], Florian Engert[1]

Affiliation

1. Department of Molecular and Cellular Biology, Faculty of Arts and Sciences, Harvard University, Cambridge, Massachusetts, 02138, USA
2. Biostatistics Center, Massachusetts General Hospital, Boston, Massachusetts, United States of America, Department of Medicine, Harvard Medical School, Boston, Massachusetts, United States of America

* Correspondence.

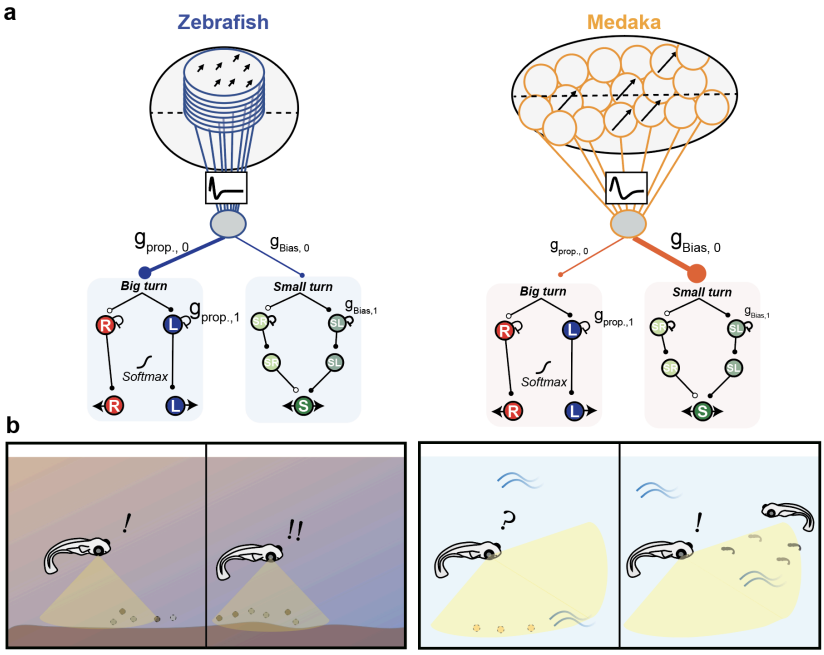

Abstract

Animals in different ecological niches have evolved different sensory capacities to detect behaviorally relevant sensory signals. How behavioral algorithms and neural networks adapt to environmental demands remains unknown. We compared spatiotemporal visual motion processing in larval zebrafish (*Danio rerio*) and medaka (*Oryzias latipes*) using whole-field motion stimuli. We find that medaka integrated motion over visual fields twice as large as zebrafish and showed greater sensitivity to peripheral visual information. Temporally, zebrafish respond robustly to stimuli with lifetimes as short as 100 ms, while medaka require lifetimes exceeding one second and retain motion information for several seconds after stimulus offset. These different time constants suggest that medaka prioritize object classification and persistence detection, such as conspecifics in structured social groups, while zebrafish specialize in rapid background motion detection for navigation in variable flow environments. Our findings demonstrate how neural computation adapts to species-specific ecological and social demands.

Introduction

Integrating and processing motion information is crucial for animals to counteract dynamically changing environmental stimuli. When animals detect external whole-field motion, they can utilize the information to adjust their orientation and locomotion to stabilize their position relative to the visual environment, a behavior known as the optomotor response (OMR) (Clark 1981); (Borst, Haag, and Reiff 2010; Alexander et al. 2022). Different environments generate distinct motion patterns, and animals have evolved specialized sensorimotor strategies to process these habitat-specific cues (Oteiza and Baldwin 2021; Dusenbery 1992). However, few studies have investigated how the behavioral algorithms and neural networks underlying these responses have co-evolved to facilitate ecological adaptation.

Motion detection involves processing information across two fundamental dimensions: the spatial and the temporal axes. Spatial integration occurs when motion stimuli appear at different scales or locations within the visual field; stimuli moving in the same direction across multiple regions summate to produce stronger responses, whereas opposing motion patterns create inhibitory interactions (Naumann et al. 2016; Wei et al. 2011). Additionally, many animals exhibit region-specific sensitivities within their visual field that reflect ecological demands (Yoshimatsu et al. 2020; Baden et al. 2013; Zimmermann et al. 2018). Temporal integration is essential for accumulating sensory evidence over time and requires neural mechanisms for information retention (Bahl and Engert 2020; Groschner et al. 2018). In natural environments, the temporal characteristics of motion stimuli provide critical contextual information: brief, randomly distributed motion may represent environmental noise, while sustained, coherent motion typically indicates the presence of objects or self-motion cues (Olveczky, Baccus, and Meister 2003). If animals have evolved in environments with distinct sensory demands, their response properties for both spatial and temporal integration should reflect these adaptations.

To explore how evolution has shaped sensorimotor transformations, we selected teleost fish larvae as model systems, leveraging their small body size and well-characterized behavioral repertoire. We compared two species with contrasting ecological niches: zebrafish (*Danio rerio*) and medaka (*Oryzias latipes*). Zebrafish naturally inhabit slow-flowing, often murky waters (Engeszer et al. 2007; Spence et al. 2006) and exhibit extended larval development with limited early mobility (Widrick et al. 2023), while medaka are found in clearer waters with relatively faster flow rates (Hilgers and Schwarzer 2019) and demonstrate immediate swimming capability upon hatching (Lucon-Xiccato et al. 2020). Their breeding habits also reflect these environmental adaptations: medaka eggs have sticky filaments around the chorions, and medaka mothers carry and glue eggs onto the root of aquatic plants after breeding (Murata et al. 2019), while zebrafish mothers drop eggs whose surface are smooth (Nasiadka and Clark 2012). These ecological and developmental differences suggest distinct evolutionary pressures on visual-motor processing. In zebrafish larvae, local light-dark moving contrasts are known to elicit robust OMR (Kist and Portugues, 2019), and the neural mechanisms underlying these responses have been extensively studied in the optic tectum and hindbrain (Bahl and Engert, 2020; Naumann et al., 2016). By contrast, previous studies in medaka have demonstrated OMR to vertical stripe patterns in adult and juvenile stages (Imada et al. 2010), and OMR assays have been utilized to assess color and contrast sensitivity in mutant and transgenic lines (Harada et al.

2019; Suzuki et al. 2024). However, the specific behavioral algorithms governing OMR in medaka larvae remain uncharacterized, making cross-species comparisons particularly valuable for understanding evolutionary adaptations.

In this study, we quantified and compared optomotor responses between zebrafish and medaka larvae across multiple stimulus conditions. Using systematic behavioral experiments, we examined spatial integration properties with spatially distinct visual stimuli and characterized temporal integration dynamics using control theory frameworks. We developed a mechanistic computational model incorporating hypothesized neural control circuits that successfully reproduces species-specific behavioral patterns and reveals distinct temporal processing strategies. Our findings demonstrate that these species have evolved different approaches to processing visual motion information, with implications for understanding how ecological pressures shape the evolution of sensorimotor control systems.

Results

Cross-species comparison in optomotor response (OMR) in teleost larvae

We compared larvae of two teleost species, zebrafish and medaka (**Figure 1a,b**), which have evolved in distinct ecological niches (**Figure 1a**). While both species can be found in rice field environments, zebrafish typically inhabit slow-flowing, often turbid waters, whereas medaka are more commonly found in clearer, faster-flowing streams. Given that adapting to environmental visual cues is crucial for larval survival, this study aimed to determine whether these species have evolved different behavioral strategies for responding to whole-field motion stimuli.

To enable meaningful cross-species behavioral comparisons, we first identified comparable developmental stages. Based on literature describing organ development (Furutani-Seiki and Wittbrodt 2004) and our observations of locomotor ontogeny, we determined that 5-6 days post-fertilization (dpf) zebrafish and 0-1 days post-hatch (dph) medaka exhibit similar swimming maturity (**Supplementary Figure 1a**). Specifically, 5–6 dpf zebrafish and 7–8 dpf (0–1 dph) medaka demonstrated comparable regular swimming patterns and were therefore used for all behavioral experiments. We utilized a behavioral assay in which visual stimuli were projected from below the experimental arena while fish swimming behavior was recorded from above (**Figure 1c**). To quantitatively assess optomotor responses, we measured turn angles as the deviation in head orientation before and after movement bouts (**Figure 1d**). While zebrafish swim in discrete bouts making turn angle calculation straightforward, medaka exhibit continuous tail undulation but also display discrete acceleration bouts during which head angle changes occur, enabling comparable measurements across species. As a complementary metric, we calculated the fraction of turns aligned with stimulus direction as the 'correct response fraction' (Harpaz et al. 2021)(Chen et al. 2021; Bahl and Engert 2020) (**Supplementary Figure 1b**).

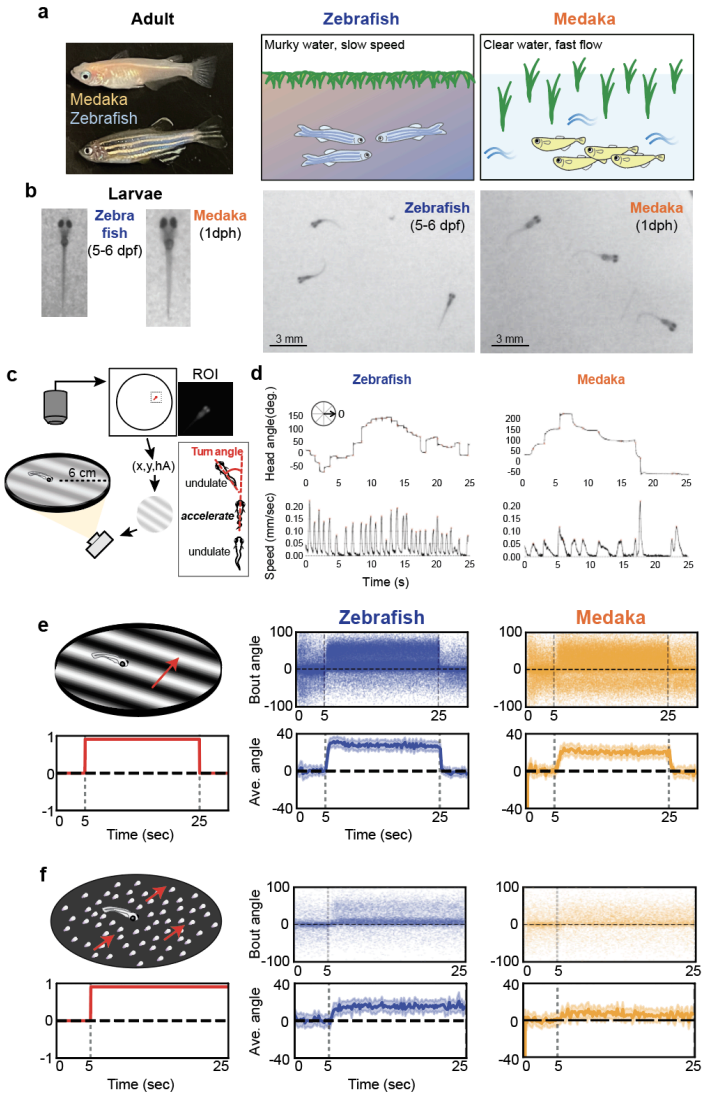

Figure 1. Comparative study of optomotor response (OMR) in zebrafish and medaka larvae

(a) Zebrafish and medaka species comparison. Adult fish (left; top: medaka, bottom: zebrafish) and schematic drawings of their natural habitats (right) are shown. Zebrafish and medaka inhabit divergent aquatic environments: zebrafish live in slow-moving, murky waters, whereas medaka inhabit rice fields and rivers with clear, fast-flowing water. **(b)** Larval specimens used in this study. Larvae at 5-6 days post-fertilization (dpf) for zebrafish and 1 day post-hatch (dph) for medaka were examined. Scale bar: 3 mm. **(c)** Free-swimming behavioral experiment rig. Individual larvae were placed in a 6 cm-radius circular arena. A high-speed camera above the dish took the whole image of the behavioral rig at 90 fps. The center of mass position (x, y) and head angle (hA) of the focal larvae are recorded. Visual stimuli were generated based on these parameters and projected from beneath the arena. **(d)** Swimming dynamics of zebrafish (left) and medaka (right) larvae. Zebrafish exhibit discrete swimming bouts alternating with interbout periods, whereas medaka demonstrate continuous undulatory swimming with rhythmic acceleration phases. Turn angles were quantified as the deviation in head angle before and after acceleration time points, as illustrated in the bottom right inset of **(c)**. **(e)** Optomotor response to whole-field sine-grating stimuli (top left). The red trace represents the temporal stimulus pattern (bottom left), where positive values indicate leftward motion and negative values indicate rightward motion. Each trial consisted of 5 s open-loop converging sine-grating baseline, followed by 20 s closed-loop sine-grating stimuli, and 5 s static grating. Turn angles for all swimming bouts are plotted (right, top row; blue:

zebrafish, orange: medaka), with averaged responses shown below (right, bottom row) (zebrafish: n=53, medaka: n=42). **(f)** Optomotor response to whole-field random dot motion stimuli (top left). Protocol identical to **(e)**: 5 s open-loop converging sine-grating baseline, followed by 20 s closed-loop random dot motion stimuli (bottom left). Individual bout turn angles (top row) and averaged responses (bottom row) are shown (zebrafish: n=21, medaka: n=32).

We characterized optomotor responses using two stimulus types: sine-wave gratings (**Figure 1e**, **Supplementary Figure 1b**) and flickering dot motion (**Figure 1f**, **Supplementary Figure 1b**). Each trial began with 5 seconds of open-loop converging motion to center the fish, followed by closed-loop whole-field motion stimuli that were locked to fish position and head angle. Both species exhibited reliable and consistent directed turning toward the direction of moving whole-field stimuli, as evidenced by changes in average turning angles (**Figure 1e,f**) and correct response fractions (**Supplementary Figure 1b**), but zebrafish generally exhibited more vigorous optomotor responses compared to medaka, as measured by both turn angle magnitude and response consistency (**Supplementary Figure 1b**). These initial observations suggested species-specific differences in visual-motor processing that warranted further investigation.

Local and global spatial integration

From our initial observations, we noticed that larval turning behavior varied systematically with distance from the arena wall. Specifically, proximity to the wall reduced the ability to execute large-angle turns in the stimulus direction, suggesting that the wall acts as a visual 'distractor' (**Figure 2a, 2b left, 2c top, 2d solid lines, 2e top**). Average turn angles were significantly higher when larvae were positioned near the center of the arena in both zebrafish (blue) and medaka (orange), and decreased progressively as fish moved closer to the wall (**Figure 2d, e, solid lines**). This pattern suggests that turning behavior is driven by the integrated motion energy within the fish's visual field, with the black arena wall apparently inhibiting turning responses by occupying visual space with non-moving dark regions. Importantly, this wall-proximity effect was more pronounced in medaka than in zebrafish, indicating species differences in spatial integration.

Notably, medaka displayed a tendency to execute turns opposite to the stimulus direction when swimming close to the wall (<30 mm) (**Figure 2c, solid line**). This paradoxical response reflects a significant number of turns away from the wall, possibly triggered by the motion stimulus' reflection off the acrylic surface of the wall whose mirrored direction contains motion energy in the opposite direction, when the wall is on the side of the fish.

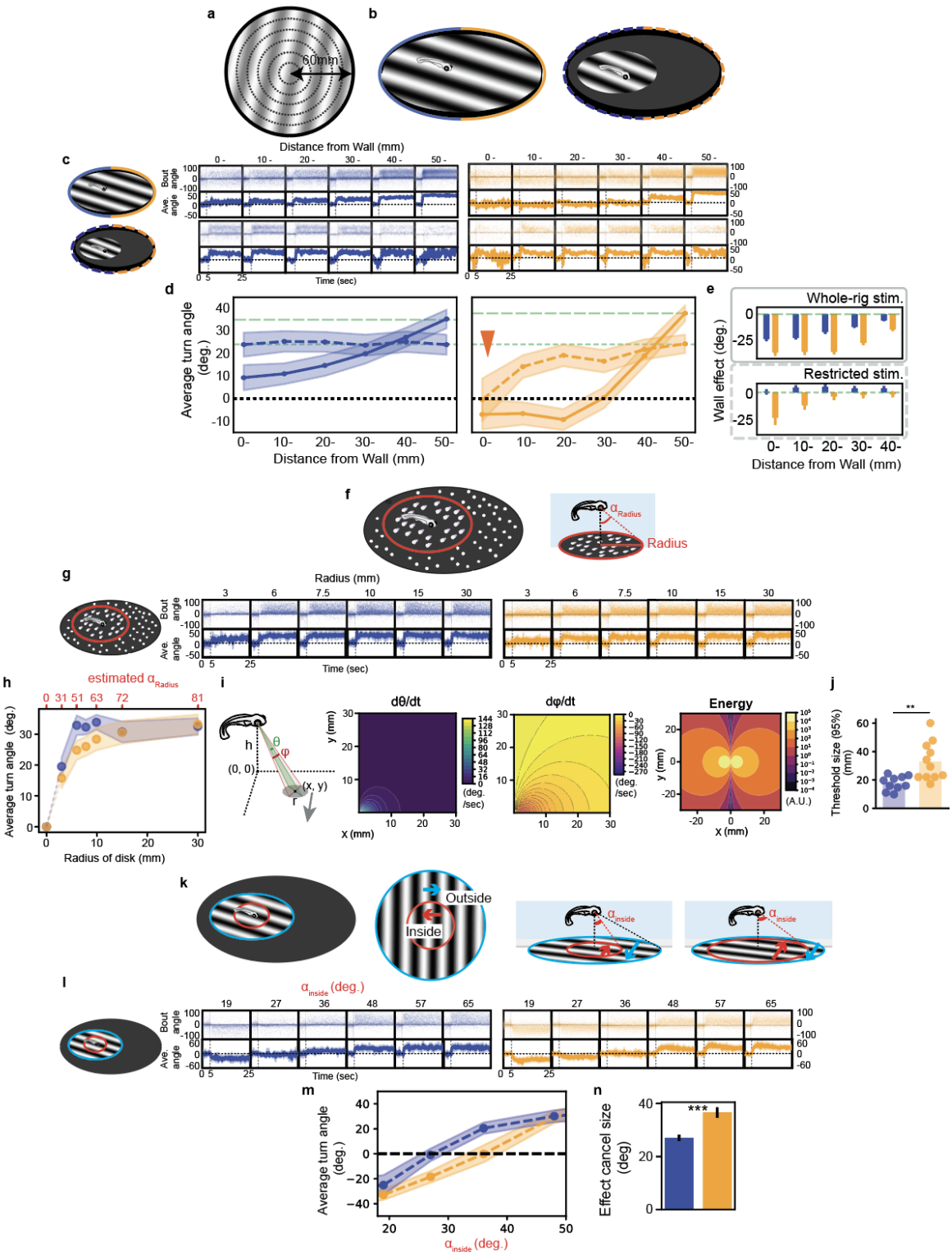

Figure 2. Spatial integration of the whole-field motion stimuli in teleost larvae

(a) Schematic of experimental arena. Turns were categorized based on distance from the wall where each turn occurred. **(b)** Sine-grating stimulus configurations: whole-field stimuli (left) or restricted area around the fish (right, 3 cm radius). **(c)** Turn responses at different distances from the wall. Raw angular data (top) and averaged turn angles across spatial bins (bottom) during trials with 5 s open-loop converging stimuli followed by

20 s closed-loop stimuli. Top rows: whole-field sine-grating stimuli (solid frames) (zebrafish n=42, medaka n=53). Bottom rows: restricted-area stimuli (dotted frames) (zebrafish n=33, medaka n=31). Blue: zebrafish, orange: medaka. **(d)** Averaged turn angles during closed-loop stimuli from (c). Solid lines: whole-field stimuli; dotted lines: restricted stimuli. Green dotted lines indicate wall-nearest area responses in each condition. Mean turning angles (± SEM) across six spatial bins from wall (bin 0) to center (bin 50). Statistical significance determined by Bonferroni-corrected t-tests following significant stimulus × spatial bin interaction in two-way mixed ANOVA (*$p < 0.05$, $p < 0.01$, $p < 0.001$). Orange arrowhead indicates persistent wall effect. **(e)** "Wall effects" calculated as deviation between each area and wall-nearest area. With whole-field stimuli, wall effects exist significantly in both species; with restricted stimuli, only medaka show significant wall effects. **(f)** Moving dots presented in disks of varying radii beneath fish, with stationary dots in surrounding areas. Visual occupying angle (α_{disk}) estimated for fish swimming 0.5 mm above sandblasted dish bottom. **(g)** Turn responses to different motion disk sizes. Raw angular data (top) and averaged angles (bottom) (zebrafish n=10, medaka n=12). **(h)** Averaged turn angles during 5-25 s across motion disk sizes. Shaded areas: standard errors. Dotted lines: fitted curves based on motion energy calculations. **(i)** Motion energy calculation for larvae at height h. Each dot at position (x, y) occupies a visual field angle (θ, φ). For x-axis motion, angle changes depend on position (left: dθ/dt, middle: dφ/dt), and motion energy (dθ/dt × dφ/dt) varies by position (right). **(j)** Larger disks produce greater turning angles, but zebrafish reach 95% maximum response at smaller sizes than medaka (zebrafish: 17.8 ± 4.8°, medaka: 32.8 ± 12.9°; Welch's t-test, p=0.0044). **(k)** Inconsistent motion stimuli with opposing directions in inner and outer regions. Response measured across different inner disk angular sizes. **(l)** Turn responses to varying inner disk sizes. Raw bout data (top) and averaged angles (bottom) (zebrafish n=6, medaka n=11). **(m)** Average turn responses versus inner disk size. Black dotted line indicates "effect cancel size" where inner and outer motions balance. **(n)** Effect cancellation size comparison. Medaka showed significantly larger cancellation angular size than zebrafish (zebrafish: 27.0 ± 1.2°, medaka: 36.6 ± 2.0°; Student's t-test, p=0.00099).

To isolate sensorimotor transformations from contextual influences, we designed stimuli where visual motion was restricted to a constrained area (~3 cm radius) centered around the fish (**Figure 2b right**). Both species showed significantly improved turning responses to such restricted sine-grating stimuli compared to whole-arena stimuli (**Figure 2c bottom, 2d dotted line**). In all panels dotted lines denote restricted area stimuli, whereas continuous lines denote whole-arena stimulation. In zebrafish, this restricted stimulus effectively eliminated the wall effect (**Figure 2d blue dotted line, 2e bottom, blue**). However, in medaka, the wall effect persisted (orange arrowhead in **Figure 2d**), as demonstrated by continued position-dependent turning behavior even against a black background where the dark bottom and walls appear as continuous darkness. These results suggest that zebrafish are less influenced by peripheral visual information compared to medaka.

To systematically examine how the two species respond to motion at different spatial scales, we measured responses to dot motion stimuli covering varying spatial extents (**Figure 2f**). To that end we projected stationary flickering dots across the entire arena, where only a subset of dots within a restricted circle moved coherently relative to the fish. This arrangement allowed us to systematically vary the size of the motion area and thereby the optical angle subtended by the motion stimulus. Analysis of response magnitude versus motion area revealed distinct spatial integration profiles (**Figure 2g, h**). Zebrafish responded robustly to moving dot stimuli even at small optical angles (20 degrees), with response rates saturating at 99% already at 40 degrees. In contrast, medaka larvae exhibited a more gradual increase in turn angles as the spatial extent of moving dots expanded. Even at 80 degrees subtended visual angles medaka only reached an estimated saturation of 95% of

turning, indicating that the effective visual angle might extend to regions above the horizontal plane (> 90 degrees).

To quantify these species differences, we calculated the motion energy of individual dots within the stimuli and integrated this energy over the motion area. We then fitted the relationship between integrated motion energy and larval turning responses to determine the spatial extent over which each species integrates motion information (**Figure 2i, Supplementary Figure 2**). By measuring the 95% threshold required to reach saturation response levels, we found that medaka demonstrated significantly broader spatial integration (threshold medaka tM = 32.8 ± 12.9 compared to zebrafish (threshold zebrafish tZ =17.8 ± 4.8, (Mean ± STD)) (**Figure 2j, Supplementary Figure 2**). This quantitative analysis confirms that medaka require motion signals from a larger spatial area to achieve equivalent behavioral responses, reflecting fundamental differences in visual-motor integration strategies between the two species.

As a final validation of species differences in spatial integration, we presented spatially conflicting whole-field motion stimuli (**Figure 2k–n**). To that end sine-grating stimuli moving in one direction were projected beneath the fish, while opposing-direction gratings were projected in the surrounding area (**Figure 2k**). By varying the inner disk size, we determined the spatial extent required for local motion to balance global motion signals. When the inner disk was small, larvae turned in the direction of the outer (global) motion. As the inner disk size increased, larvae switched to following the inner (local) motion direction. The critical transition occurred at 23 degrees optical angle in zebrafish but at 39 degrees in medaka (**Figure 2m, n**), confirming that medaka require a larger local motion area to override global motion signals.

Together, these data demonstrate that medaka have broader spatial integration compared to zebrafish, consistent with a significantly wider field of view for motion processing.

Temporal integration of flickering dot motion stimuli

Next, to investigate species differences in temporal motion integration, we employed random flickering dot stimuli and systematically varied stimulus lifetimes (**Figure 3**). We presented 500 small dots beneath freely swimming larvae, with dots moving either leftward or rightward according to the fish's head orientation. Each dot had a limited lifetime and appeared at random positions within the restricted area beneath the fish (**Figure 3a**). Consistent with previous findings (Bahl and Engert, 2020), zebrafish responded robustly to dot motion stimuli even with very short lifetimes (100 ms) (**Figure 3b, c, blue**). In contrast, medaka exhibited significantly smaller turning responses to short-lifetime dot motion stimuli (**Figure 3b, c, orange**). However, as dot lifetime increased, medaka correct response ratios progressively improved to levels comparable to zebrafish. To quantify these temporal dynamics, we fitted exponential growth functions to the relationship between dot lifetime and response magnitude. This analysis revealed significant differences in temporal integration constants between species (**Figure 3d**). Zebrafish demonstrated rapid response saturation with integration times as short as 0.091 ± 0.033 (Mean ± STD) seconds, while medaka required longer stimulus durations (2.26 ± 0.77) to achieve equivalent response levels.

Based on these temporal integration profiles, we propose distinct underlying neural architectures. Zebrafish appear capable of rapidly integrating short-lifetime motion stimuli, potentially through retinal ganglion cells or downstream visual areas with larger receptive fields that enable efficient temporal summation of whole field motion stimuli. In contrast, medaka's requirement for longer stimulus durations to achieve strong responses suggests a visual system composed of retinal ganglion cells with smaller receptive fields that integrate motion stimuli through longer temporal filters (**Figure 3e**). This architectural difference may reflect evolutionary adaptations to their respective visual environments, with zebrafish optimized for rapid motion detection in turbid waters and medaka specialized for sustained motion tracking in clearer environments.

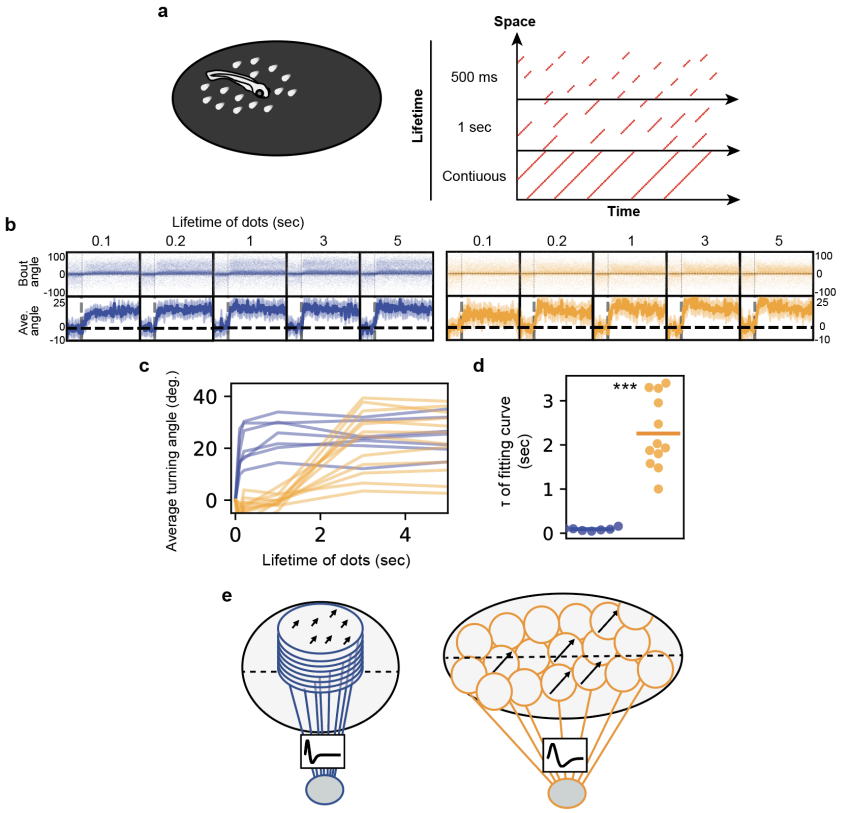

Figure 3. Comparative study in temporal domain in OMR using flickering dot motion

(**a**) Flickering dot motion stimuli presented to free-swimming larvae in a restricted area beneath the fish (left). Dots have defined lifetimes and random spatial locations (spatiotemporal patterns shown on right). (**b**) Turn responses to varying dot lifetimes during trials. Raw bout data (top) and averaged turn angles (bottom). Blue: zebrafish (n=7), orange: medaka (n=12). (**c**) Average turn angle increases more slowly in medaka (orange) than zebrafish (blue). Solid lines: experimental data; dotted lines: fitted exponential curves. (**d**) The time constant of the fitting curve was shown. The values of each fish are shown dots and the averages are shown in horizontal lines. The time constants were significantly larger in medaka than zebrafish (zebrafish: 0.09 ± 0.01, medaka: 2.26 ± 0.23 (Mean ± SEM), Welch's t-test, p=0.000001). (**e**) Schematic model of how visual stimuli could be processed in zebrafish (left) and medaka (right) larvae. In zebrafish, we hypothesized that the motion stimuli is averaged globally in a big receptive field (blue circle) and the top part of the retina. On the other hand, in medaka, we hypothesized that the motion stimuli is processed in a local receptive field which is tiled up in a bigger retina and temporally filtered and passed to the averaging step.

Divergent temporal filters uncovered by pulsed motion stimuli

To quantitatively estimate temporal filter properties for motion processing, we presented unidirectional motion pulses to fish larvae of both species and analyzed the dynamics of turning responses during and after the motion pulse (**Figure 4**). Using pulse stimuli of varying durations (**Figure 4a, 4b, Supplementary Figure 4**), we characterized both response onset and decay kinetics.

Analysis of average turning responses revealed similar onset time constants across species (zebrafish: 0.48 ± 0.02 s, medaka: 0.55 ± 0.06 s), but significantly longer decay time constants in medaka (1.24 ± 0.14 s) compared to zebrafish (0.41 ± 0.02 s) (**Figure 4c**). This difference suggests that while both species initiate responses with comparable speed, medaka maintain motion-driven turning behavior for substantially longer periods after stimulus offset.

Fish larvae exhibit two distinct types of turning behavior—small turns and big turns—which are readily distinguishable in turn angle distributions. To investigate the temporal dynamics of these behavioral components separately, we generated turn angle distributions for each 100 ms time bin during stimulus presentations (**Figure 4d, 4e**) and fitted them with three-component Gaussian distributions. We extracted the difference between big left and big right turn frequencies as the “big turn proportion” (**Figure 4e middle, purple**) and the mean bias angle of small turns as the “small turn bias” (**Figure 4e bottom, green**). Exponential curve fitting of both “big turn proportion” and “small turn bias” revealed that rise and decay time constants of big turns were not significantly different between zebrafish and medaka (**Figure 4f, top left**). This suggests that the neural circuits processing signals inducing large-amplitude turning maneuvers have similar temporal characteristics across species, potentially reflecting conserved mechanisms for rapid escape or orientation responses.

In contrast, small turns displayed markedly different temporal profiles. Both species showed longer rise time constants for small turns (zebrafish 0.701 ± 0.04 s, medaka 0.894 ± 0.096 s) compared to big turns (zebrafish: 0.302 ± 0.004 s, medaka: 0.363 ± 0.014 s) (**Figure 4f, left column**), indicating low pass filtering of signals inducing small turns. Most strikingly, decay time constants for small turns exceeded rise time constants in both species, but medaka exhibited significantly longer small turn decay constants compared to zebrafish (zebrafish: 1.130 ± 0.04 s, medaka: 2.041 ± 0.059 s) (**Figure 4f**). This represents a remarkable species difference, with medaka small turn responses persisting nearly twice as long as those in zebrafish. Given that neural spiking occurs on millisecond timescales, this ~1-second difference in behavioral persistence suggests fundamentally different temporal integration mechanisms underlying small turn control between the two species.

Since small turns play a more dominant role in medaka swim behavior than in zebrafish, this extended time constant becomes prominent also in the overall average turn angle (**Figure 4c**), which relaxes in medaka with a time constant that is three times longer than that of zebrafish (medaka: 1.24 ± 0.14 s, zebrafish: 0.41 ± 0.02 s).

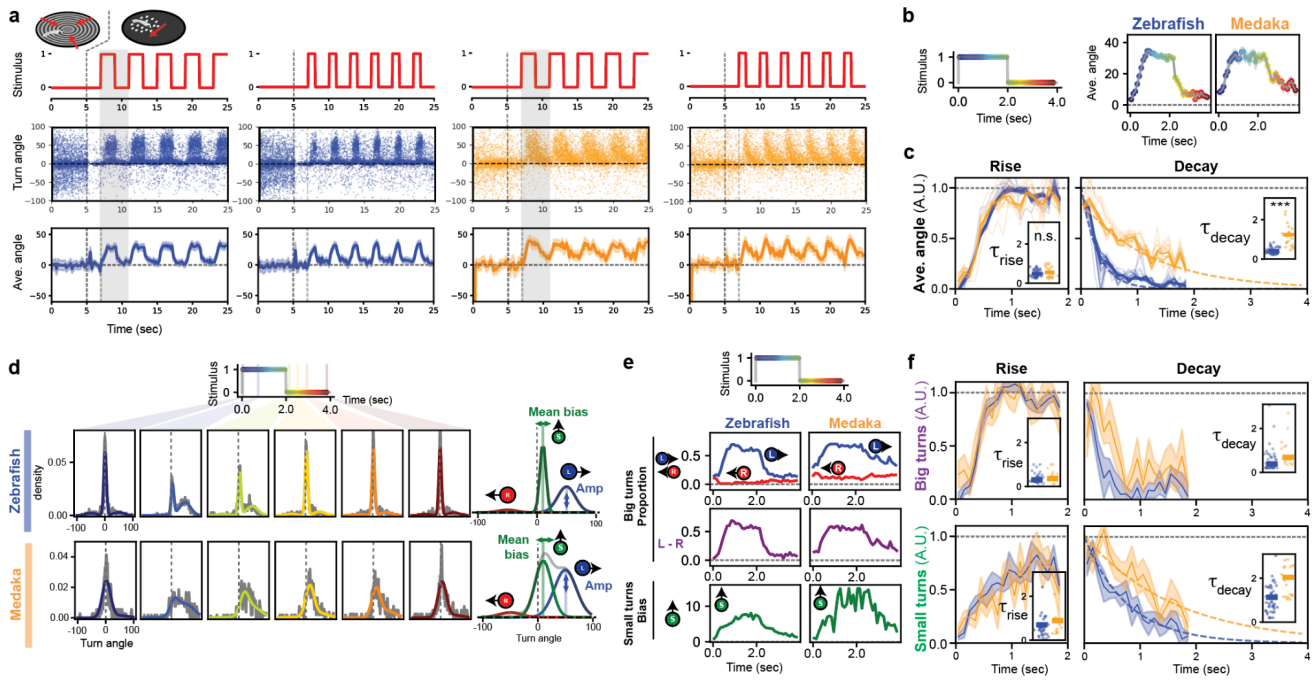

Figure 4. Divergent responses to unidirectional motion pulse stimuli reveal species-specific temporal dynamics.

(a) Turn dynamics to unidirectional pulse stimuli. Trials begin with 5 s converging stimuli (black dotted lines), followed by square-wave motion (red trace, top). Individual (middle) and averaged (bottom) turn angles for zebrafish (blue, n=52) and medaka (orange, n=21; shaded areas: standard error). **(b)** Single-cycle stimulus-response analysis. One complete cycle is shown for zebrafish (left) and medaka (right). Dot colors correspond to temporal bins. **(c)** Normalized pulse responses and kinetics. Rise time constants: no species difference (zebrafish: 0.48 ± 0.02 s, medaka: 0.55 ± 0.06 s; p=0.52, n.s., mean ± SEM; Mann-Whitney U test). Decay time constants: significantly longer in medaka (zebrafish: 0.41 ± 0.02 s, medaka: 1.24 ± 0.14 s; $p=4.0\times10^{-10}$). Blue: zebrafish, orange: medaka. Thin lines represent temporal dynamics of normalized average turn angles for individual fish; thick lines represent population averages. Inset dot plots show individual fish time constants for rise and decay phases. **(d)** Three-component Gaussian decomposition: large leftward (blue), large rightward (red), and small turns (green). Temporal dynamics in 100 ms bins with fitted curves overlaid. **(e)** Temporal evolution of behavioral components. Large-turn amplitudes (top), small-turn means (bottom), and large-turn asymmetry (left minus right amplitude, middle, purple). **(f)** Species comparison of temporal dynamics. Time constants (mean ± SEM): zebrafish large turns (rise: 0.302 ± 0.004 s, decay: 0.384 ± 0.037 s), zebrafish small turns (rise: 0.701 ± 0.04 s, decay: 1.130 ± 0.04 s), medaka large turns (rise: 0.363 ± 0.014 s, decay: 0.684 ± 0.141 s), medaka small turns (rise: 0.894 ± 0.096 s, decay: 2.041 ± 0.059 s). Zebrafish n=53, medaka n=20.

Alternating stimuli

The prolonged decay kinetics observed in medaka's average turning responses and small turn components suggested enhanced signal retention capacity compared to zebrafish. To test this hypothesis systematically, we presented alternating motion stimuli across a range of frequencies and performed frequency-domain analysis.

Even in zebrafish, which showed relatively short decay time constants, the response curves deviated from pure sinusoidal patterns, exhibiting steep slopes that indicated nonlinearities in the

underlying control systems (**Figure 5a,b**). Frequency-amplitude analysis revealed distinct processing strategies between species: zebrafish demonstrated approximately linear amplitude decay with increasing stimulus frequency, while medaka exhibited exponential amplitude decay (**Figure 5c**). This difference suggests fundamentally different frequency-dependent filtering mechanisms.

To dissect the temporal dynamics of big turns and small turns separately, we fitted three-component Gaussian distributions to turn angle distributions within each 200 ms time bin (**Figure 5d, Supplementary figure 5**). Frequency-amplitude analysis of these components revealed species-specific patterns. Zebrafish showed relatively linear amplitude decay across frequencies for both big turns and small turns (**Figure 5e, left blue**), indicating uniform frequency processing across behavioral components. In contrast, medaka exhibited more complex frequency dependencies. Most notably, medaka big turns showed amplitude peaks at lower stimulus frequencies (~0.5 Hz) (**Figure 5e, left orange**), suggesting resonance or optimal frequency tuning in their large-amplitude turning system.

Frequency-phase analysis provided additional insights into temporal processing mechanisms. For big turns, zebrafish and medaka showed no significant phase differences across frequencies, consistent with the similar time constants observed for big turn responses to unidirectional pulse stimuli. However, small turn phase analysis revealed substantial differences between species (**Figure 5f, right**), with medaka showing significantly larger phase lags that increased with frequency. This pattern is consistent with the much longer decay time constants observed for medaka small turns in the pulse stimulus experiments, confirming that species differences in temporal integration are primarily mediated through small turn control mechanisms rather than big turn systems.

These frequency-domain results support a model where medaka have evolved slower temporal integration for fine motor adjustments (small turns) while maintaining rapid response capabilities for large corrective maneuvers (big turns), potentially reflecting adaptations to their clearer, more spatially complex visual environments.

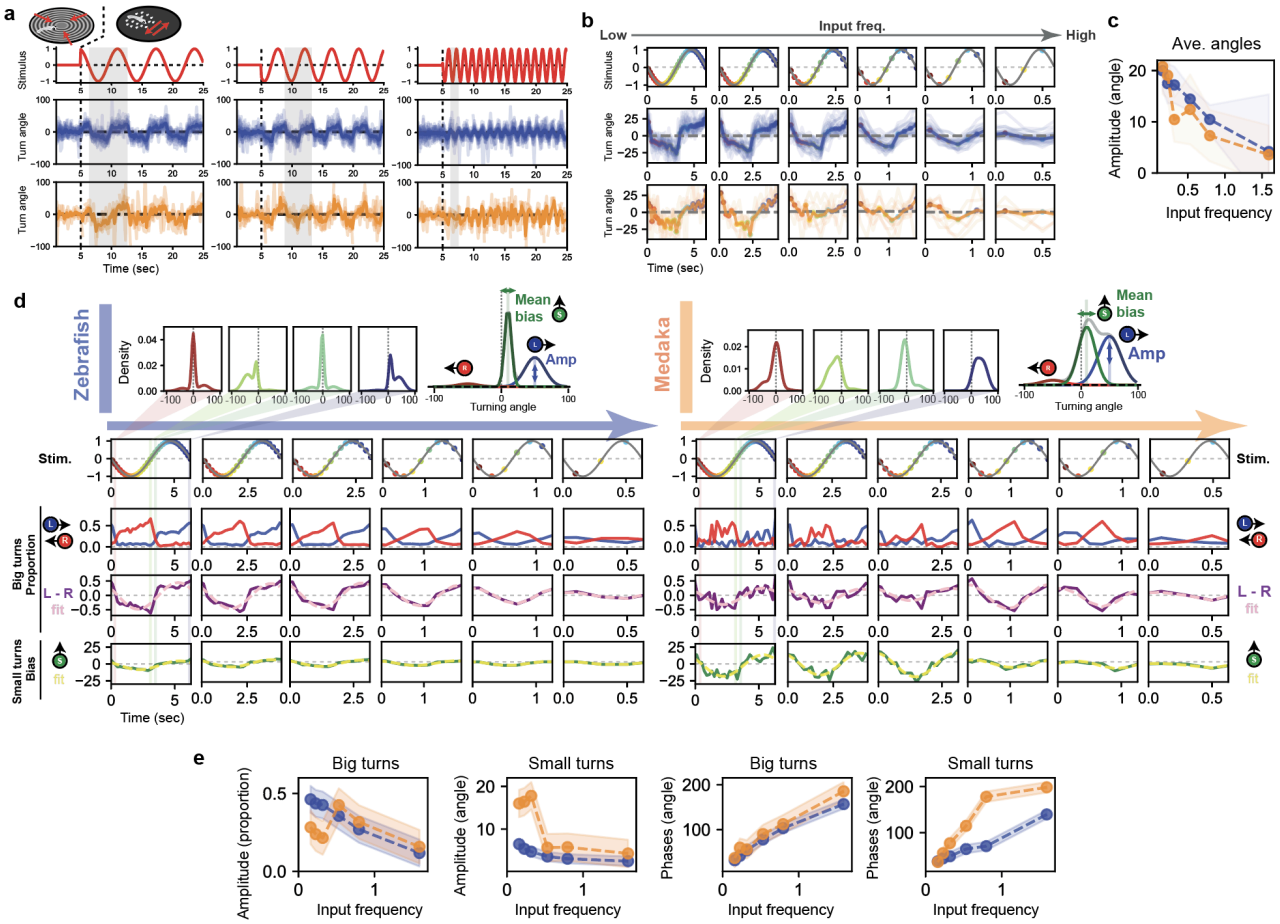

Figure 5. Optomotor response to the alternating stimuli

(a) Turn dynamics to alternating stimuli. Each trial begins with converging stimuli for 5 seconds (indicated by black dotted lines), followed by presentation of moving dots that alternate between leftward and rightward motion with velocities following a sinusoidal pattern (red, top row). **(b)** Frequency-response characterization. Average turn angles plotted with colored dots indicating time bins within cycles and corresponding responses. Input and response frequencies show a linear relationship. **(c)** Response amplitude analysis. Amplitudes of fitted sine waves plotted versus stimulus frequency. **(d)** Turn angle distribution analysis within cycles. Fitted curves for 200 ms bins during one complete cycle (2π) for zebrafish (left) and medaka (right). Line colors correspond to temporal positions. Three Gaussian components are fitted: large rightward (red), large leftward (blue), and small turns (green) (top right). Amplitudes of large-turn distributions (third row) and means of small-turn distributions (bottom, green) across cycles. Large-turn asymmetry dynamics (left minus right amplitude, fourth row, purple) and small turns fitted with sine waves (dotted pink: large turns, dotted yellow: small turns). **(e)** Frequency-domain analysis of behavioral components. Following sine wave fitting, amplitude and phase of large and small turn components plotted to characterize frequency-amplitude and frequency-phase response profiles. Shaded regions: confidence intervals (blue: zebrafish, orange: medaka).

Mechanistic models reproduce species-specific temporal dynamics

To test our understanding of the underlying neural mechanisms, we developed a mechanistic computational model that simulates the temporal dynamics of optomotor responses using the Euler

method (**Figure 6a**). The model implements separate control systems for big turns (proportional control) and small turns (bias control), each governed by input gain (g_0) and decay rate (g_1) parameters. Based on observations from alternating stimuli experiments, we also incorporated a softmax function to capture the nonlinear response characteristics observed in both species.

Analysis of the three-component Gaussian distributions revealed that medaka small turns contribute substantially more to average turning behavior than zebrafish small turns, a feature we incorporated into our modeling framework. Parameter sensitivity analysis demonstrated how variations in big turn proportions (purple) and small turn bias (green) influence overall behavioral outputs across different parameter ranges (**Figure 6b**).

Fitting the model to experimental data from both species revealed key parameter differences (**Figure 6c**). Most notably, decay rates (g_1) were consistently lower in medaka compared to zebrafish for both big turn and small turn control systems. This finding directly corresponds to the longer temporal integration observed in medaka across multiple experimental paradigms, providing mechanistic support for species differences in motion processing persistence.

To test the model, we fitted parameters based on the unidirectional stimulus responses (Figure 4) and tested the model by predicting responses to alternating stimuli (**Figure 5d, 6d**). Frequency domain analysis applied to these predictions confirmed most key experimental features **(Figure 5e, 6e)**. Specifically we could capture the steep exponential decay in small turn frequency-amplitude responses observed in medaka, and a more linear decay in those of zebrafish. We also captured the progressive phase delay with increasing input frequencies in both turn modes in zebrafish. However, the model failed to capture the transient increase in big turns at intermediate frequencies in medaka. In addition, the persistent high amplitude in small turns for the lower frequencies is not captured by the model who predicts a consistent and exponential decrease in small turn bias with increasing stimulus frequencies.

These modeling limitations suggest the presence of more complex, frequency-dependent mechanisms that are not captured by simple first-order linear dynamics. Specifically, the discrepancies point toward potential behavioral switching between big turn and small turn control systems depending on input frequency, with medaka possibly employing different processing strategies at low versus high frequencies. This frequency-dependent mode switching could represent an adaptive mechanism for optimizing responses to different timescales of environmental motion, warranting future investigation of more sophisticated control architectures.

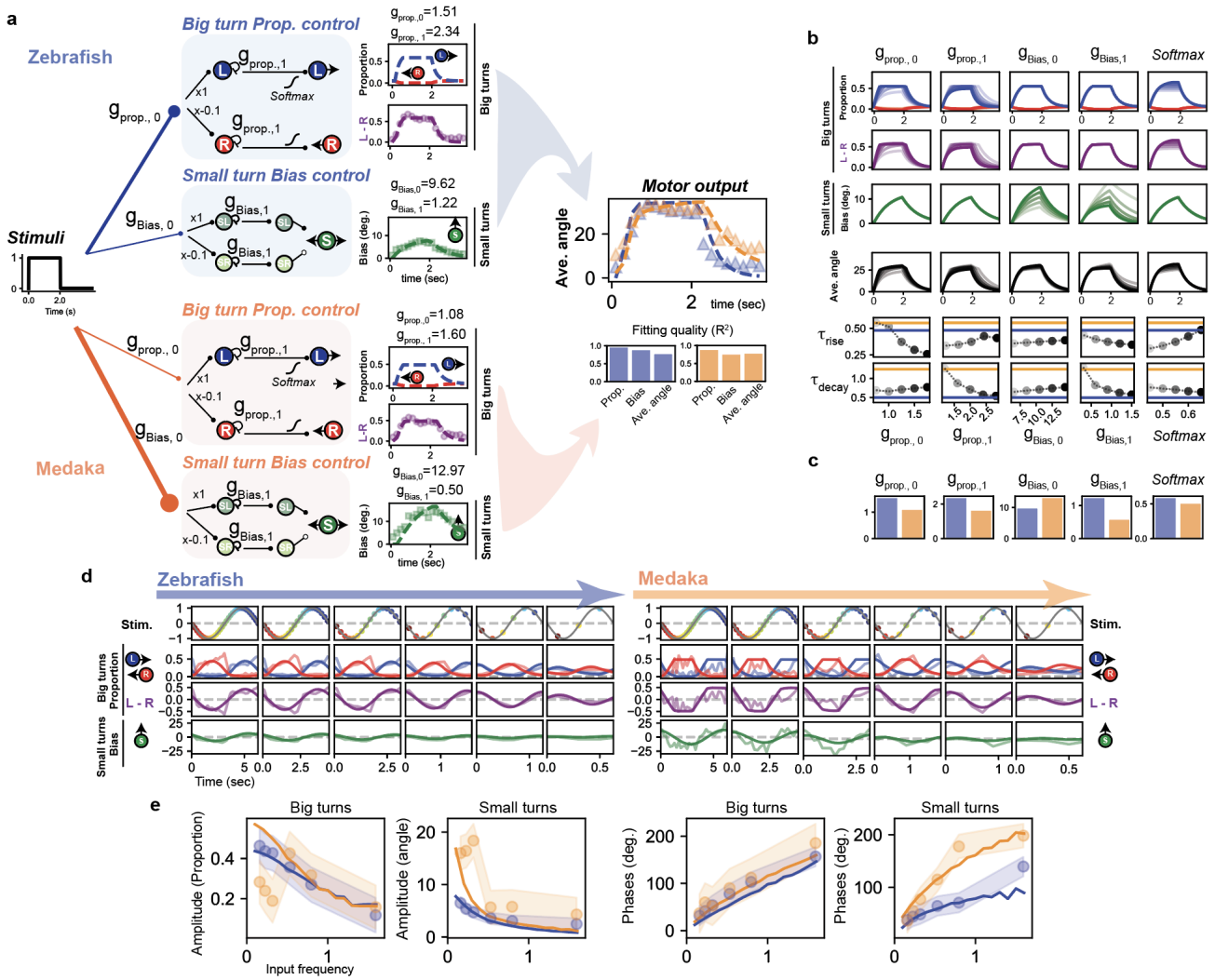

Figure 6. Temporal integration model captures species-specific optomotor responses

(a) Model architecture and fitting. Schematic shows sensorimotor control for zebrafish (blue) and medaka (orange). Visual input drives two pathways: proportion control (big turn probabilities) and bias control (small turn direction). Each implements first-order dynamics with gain (g0) and decay (g1), followed by saturation. Components shown: big turns left (blue), right (red), difference (purple), and small turn bias (green). Fitted parameters displayed above plots. Dashed lines: model predictions; dots: experimental data. Average angles (right) emerge from component combinations. Bar graphs show R^2 fitting quality. **(b)** Parameter sensitivity analysis. Model responses across parameter ranges (proportion gain g_0, decay g_1, bias gain fg_0, decay fg_1, saturation). Top: temporal dynamics with line shading corresponding to parameter values (x-axes, bottom). Bottom: rise and decay time constants versus parameters. Horizontal lines: experimental values (blue: zebrafish, orange: medaka). **(c)** Species-specific parameter estimates. Fitted values reveal distinct temporal processing strategies between species. **(d)** Simulated dynamics for alternating stimuli using parameters from (c). Experimental data from Figure 5 (shaded lines) compared to simulations (darker lines). **(e)** Frequency domain validation. Model predictions (dashed) using parameters from (c). Amplitude and phase responses versus frequency for big turn difference and small turn components. Experimental data (shaded: mean ± CI) validate predictions, revealing species differences: zebrafish show linear amplitude decay while medaka exhibits sharp cutoff around 0.5 Hz.

Discussion

In this study, we compared spatiotemporal integration of whole-field motion stimuli between zebrafish and medaka larvae, revealing substantial differences in both spatial and temporal processing domains. Our findings demonstrate that medaka exhibit broader spatial integration with larger fields of view, while zebrafish respond preferentially to motion directly beneath their bodies. Additionally, temporal analysis revealed that while both species show similar response onset kinetics, medaka display significantly longer response persistence, indicating enhanced temporal retention mechanisms at the expense of slower response times to quickly varying stimuli. These species-specific differences reflect distinct evolutionary adaptations to their respective ecological niches and social behaviors.

Spatial domain of the optomotor response

Our spatial domain analysis revealed that zebrafish primarily detect and process stimuli beneath their bodies, while medaka demonstrated broader spatial integration that extended to larger motion areas, possibly extending above the horizontal plane. This difference was particularly evident in wall-proximity effects, where medaka showed dramatic reductions in correct turning responses when swimming near arena boundaries, suggesting attention switching across wider vertical axes. These spatial integration differences could arise from several sensory and neural mechanisms, including differences in eye position, retinal organization, or receptive field properties of retinofugal targets. Indeed, it is reported that arrangement and distribution patterns of photoreceptors are different between species (Tohya, Mochizuki, and Iwasa 2003; Sato et al. 2016).

The enhanced sensitivity to peripheral visual information in medaka may reflect several evolutionary adaptations. First, medaka's clear-water habitat likely favored the evolution of broader visual processing capabilities, enabling detection of objects and conspecifics across larger spatial scales (Marshall 2017). Second, medaka's more pronounced schooling behavior (compared to zebrafish's shoaling) may require enhanced peripheral vision for monitoring neighboring individuals and maintaining group cohesion. Indeed, cichlid fish’s behavioral study shows that high water turbidity decreases fish collective behavior (Michael, Patman, and Lutnesky 2021).

Temporal Processing Reveals Distinct Object Detection Strategies

Our flickering dot experiments revealed striking species differences also in temporal integration requirements. Zebrafish achieved maximal performance with very short dot lifetimes (≤200 ms), consistent with previous findings (Bahl and Engert, 2020), while medaka performance continued to improve until dot lifetimes exceeded 2 seconds. These findings suggest fundamentally different sensory processing strategies. Zebrafish appear optimized for rapid detection of transient motion signals, potentially through retinal ganglion cells or downstream visual areas with larger receptive fields and shorter temporal integration windows (Wang et al. 2020). In contrast, medaka seem specialized for detecting persistent motion signals, possibly through smaller receptive fields with longer temporal filters. This temporal selectivity in medaka may represent an adaptation for object permanence detection—the ability to track objects that persist in the visual field, which would be particularly valuable for social species that need to maintain awareness of conspecifics (Ochiai et al. 2013; Isoe et al. 2016).

Component-Specific Temporal Dynamics Reveal Dual Control Systems

Our analysis of pulse stimuli revealed asymmetric temporal dynamics with longer decay than rise times, captured in our model through nonlinear saturation functions. Critically, decomposition into behavioral components revealed that small turns exhibited much longer time constants than big turns in both species. The dramatically longer small turn decay times in medaka (≈2 seconds) compared to zebrafish (≈1 second) suggest species-specific adaptations in fine motor control systems. This prolonged persistence in small turn responses would facilitate sustained course corrections and precise navigation, consistent with medaka's schooling behavior and structured flow environments. The shorter persistence in zebrafish small turns enables rapid disengagement and course corrections, suitable for variable, unpredictable environments.

These findings align with proposed neuroanatomical substrates, where separate neural systems control different types of motor outputs. In particular, the mesencephalic locomotor region, and the nucleus of the medial longitudinal fasciculus (nMLF) neurons in the reticulospinal projection specifically regulate small turns (Carbo-Tano et al. 2023; Rajan et al. 2022; Thiele, Donovan, and Baier 2014). Future investigations should examine how these neural populations differ between species to understand the circuit-level mechanisms underlying temporal processing differences.

Evolutionary and Social Implications

These temporal processing differences between species have important implications for understanding the evolution of social behavior and ecological adaptation. Medaka's temporal persistence mechanisms appear well-suited for schooling behavior, where sustained directional commitment by individuals promotes group cohesion. Once a school initiates movement, individual fish maintain that direction long enough for collective motion to emerge (Leem et al. 2012). In contrast, zebrafish's broadband, linear responses enable independent maneuvering and individual flexibility, consistent with their looser shoaling behavior.

The frequency-dependent processing strategies also reflect different ecological pressures. Medaka's optimization for slow, persistent changes suggests adaptation to predictable, structured flow environments like rivers, where sustained responses to environmental motion cues are beneficial. Zebrafish's emphasis on rapid, transient responses appears suited for variable, unpredictable environments where quick individual adjustments are prioritized over sustained group movements.

Mechanistic Model Reveals Neural Computational Principles

Our mechanistic computational model successfully captured the key species differences through simple parameter variations in gain and decay rates. The model's ability to reproduce temporal dynamics while failing to capture certain frequency-domain features (particularly medaka's low-frequency amplitude patterns) suggests the presence of additional complexity, possibly including frequency-dependent behavioral switching between control systems.

The model provides a framework for generating testable hypotheses about neural circuit properties. The longer decay rates in medaka suggest either enhanced recurrent connectivity or different neuromodulatory influences compared to zebrafish. Future electrophysiological investigations and connectomic analysis should examine these possibilities to validate the computational principles identified through behavioral analysis.

Our findings demonstrate that zebrafish and medaka have evolved fundamentally different strategies for processing visual motion information, reflecting adaptations to distinct ecological niches

and social behaviors. These differences operate across multiple levels—from spatial integration ranges to temporal persistence mechanisms—and suggest that seemingly similar behaviors can emerge from markedly different neural computations. Understanding these species-specific processing strategies will provide deeper insights into the evolutionary pressures that shaped these divergent sensorimotor adaptations.

Methods

Ethics statement

All experiments followed institution IACUC protocols as determined by the Harvard University Faculty of Arts and Sciences standing committee on the use of animals in research and teaching. The animal experimentation protocols, 25-03 and 22-04 were submitted and approved by this institution's animal care and use committee (IACUC). This institution has Animal Welfare Assurances on file with the Office for Laboratory Animal Welfare (OLAW), D16-00358 (A3593-01).

We followed the ARRIVE guideline 2.0; the sample size is described in the method section. Inclusion and exclusion criteria are also mentioned in the method section. For each experiment, different visual stimuli were shown in random order. Data was analyzed by blinded and masked.

Fish maintenance

Wild-type zebrafish (WIK strain) and medaka (dr-R strain) were used in this study. Embryos were incubated at 27 °C. Zebrafish hatched within 2–3 days, while medaka hatched after 7–8 days. Prior to hatching, embryos of both species were maintained in embryo water supplemented with methylene blue. After hatching, larvae were reared exclusively in filtered fish facility water (200 nm pore size), with water changes every other day. Based on published literature and the timing of locomotor development, experiments were conducted on zebrafish at 5–6 days post fertilization (dpf) and on medaka at 1 day post hatch (dph), unless otherwise specified.

Free-swimming behavioral experiments

Free-swimming behavioral experiments were conducted on fish larvae following previously established protocols (Bahl and Engert, 2020; Harpaz et al., 2021; Krishnan et al., 2023). Briefly, behavior was recorded at 90 frames per second using an overhead camera (Grasshopper3, FLIR). Sandblasted dishes (radius: 6cm) were used to present visual stimuli to the larvae. To extract behavioral features, the mode image of the first 1-minute segment of each recording was subtracted, allowing the center of mass and head angle of the focal fish to be tracked at 90 frames per second. Each experimental epoch began with a 5-second presentation of an open-loop converging stimulus, followed by 20 seconds of closed-loop visual stimulation. Visual stimuli were projected from below at 60 frames per second using an AAXA P300 projector. A single trial consisted of a randomized sequence of different visual stimuli, and each experiment included 15 repeated trials.

Visual stimuli

Visual stimuli were projected from below the behavioral rig and programmed in Python using the Panda3D package. Each epoch began with a 5-second open-loop presentation of converging stimuli (speed: 0.15, wavelength: 0.15, contrast: 1). The luminance of the stimulus, represented as a grayscale value C, was defined by the equation (r: radial position in the disk, t: time, v: velocity, K: constant):

$$C = 0.5\sin\left(\frac{2\pi(r+tv)}{\lambda}\right)K + 1.0$$

Following the open-loop phase, closed-loop stimuli were presented for 20 seconds. These included either sine-grating or random dot motion stimuli.

For sine-grating stimuli (speed: 0.15, wavelength: 0.15, contrast: 1), the luminance C was defined as:

$$C = 0.5\sin\left(\frac{2\pi(x-offset)}{\lambda}\right)K + 1.0$$

where x is the position of the fish. Random dot motion stimuli (Figure 3) were generated following Bahl and Engert (2020). For restricted stimuli, the visual stimulus disk was reduced to half the radius (number of dots: 400). During closed-loop presentation, the stimulus disk rotated in real time based on the fish's measured head angle. For whole-field stimuli (Figures 1 and 2), one of four motion directions (forward, leftward, rightward, or backward) was randomly selected and shown. In the restricted condition (Figure 2), the stimulus disk was scaled to half the rig size and centered on the fish's center of mass. The area outside the disk was black. In the variable-disk-size dot motion stimuli (Figure 2f–j), dot density and size were kept constant. For the inconsistent stimuli (Figure 2k–n), the outer disk had a radius of three-quarters of the full field, and an inner disk displayed a sine-grating moving in the opposite direction. The size of the inner disk was randomly chosen, and each fish experienced 15 trials. In Figure 3, the lifetime of dots was randomly chosen from the set [100 ms,500 ms,1 s,2 s,4 s,10 s][100 ms, 500 ms, 1 s, 2 s, 4 s, 10 s], while keeping the total number of visible dots constant throughout the session. For the pulse stimuli (Figure 4) and alternating stimuli (Figure 5), dot stimuli had a fixed lifetime of 20 seconds. In pulse stimuli experiments, the 5-second converging stimulus was followed by a 2-second rest period, after which a series of pulse and rest periods was presented. Ten stimulus conditions (combinations of five pulse durations and two rest durations) were randomly ordered per trial. Each fish experienced 15 trials. In the alternating stimuli experiment (Figure 5), leftward and rightward dot motion pulses were shown alternately. The speed of dot motion followed a sine-wave profile.

Data inclusion and exclusion criteria

For the free-swimming behavioral experiments shown in Figure 1 and Figure 2a, all fish were included in the analysis. However, we observed that fish swimming near the walls exhibited reduced responses to motion stimuli. Therefore, for the experiments shown in Figures 3–5, we excluded fish that tended to swim near the walls. Specifically, we calculated the average distance between each fish's position and the center of the arena across the entire experiment. Fish with an average distance greater than 3.5 cm were excluded from the analysis.

Calculating turning angle in larval teleosts & ratio of correct turn

To quantify turning behavior in larval fish, we first measured the displacement of the center of mass over time to compute swimming speed. Peaks in the speed profile were detected and defined as "turn" events. For each detected turn, the change in head angle before and after the speed peak was calculated as the turn angle. Throughout the experiments, we recorded the turn angle, timing, and spatial position of each turn within the behavioral arena for further analysis. Turn angles were averaged across all turning events that occurred during sine-grating or dot motion stimuli, computed in 100 ms time bins. Both leftward and rightward motion stimuli were presented during the experiments. For presentation purposes, responses to rightward stimuli were mirrored and combined with responses to leftward stimuli to generate a unified representation. To calculate the correct turning ratio, a turn was classified as a "correct turn" when the sign of the fish's turning angle matched the direction of the visual motion stimulus (leftward: positive; rightward: negative). The correct ratio was defined as the number of correct turns divided by the total number of turns. A correct ratio of 0.5 indicates random turning behavior.

Calculation of motion energy in different size of motion disks and estimation of thresholds in teleost larvae

To estimate and compare motion energy across different sizes of dot-motion disks (Figure 2f–j), we first computed the retinal occupancy of each dot (radius: *r*) located at position (*x*, *y*) for a fish swimming at height *h*. Specifically, we calculated the horizontal (φ) and vertical (θ) angular spans subtended by each dot on the retina (see Supplementary Figure 2a,b). We then computed the rate of change of these angles (dφ/dt and dθ/dt) over time as the dots moved along the *x*-axis (Supplementary Figure 2b). The motion energy contributed by each dot in the *x*–*y* plane, denoted as $E_{abs}(x, y)$, was defined as the product of dφ/dt and dθ/dt (Supplementary Figure 2c). The total motion energy within a given motion disk (radius: *R*), denoted as $E_{total}(R)$, was calculated by summing the local motion energy over the entire disk area (Supplementary Figure 2d). To estimate motion sensitivity thresholds in zebrafish and medaka larvae for different disk sizes, we fit the behavioral responses to an exponential curve. The threshold was defined as the radius at which the behavioral response reached 95% of its asymptotic (maximum) value.

Estimation of time constants

To investigate species differences in temporal integration of motion stimuli (Figure 4), we presented unidirectional visual pulse motion stimuli to free-swimming zebrafish and medaka larvae and quantified their turning responses. Each trial began with 5 seconds of open-loop converging stimuli, followed by a randomly selected combination of motion and resting durations. This pulse pattern was repeated for a total of 25 seconds. Motion durations were 5, 2, 1, or 0.5 seconds, and resting durations were either 2 or 0.25 seconds. Each fish underwent 15 trials.

To analyze the temporal dynamics of the turning response, all turns from the repeated pulses were aggregated per fish and treated as a single composite sequence. The rise and decay phases of the averaged turn angle were then quantified by fitting exponential functions and extracting the time constant (τ) as follows:

$$\text{Rise}: \quad A \cdot \left(1 - e^{-\frac{(x-t_0)}{\tau}}\right) + \text{offset}, \quad \text{Decay}: \quad A \cdot e^{-\frac{(x-t_0)}{\tau}} + \text{offset}$$

where *A* is the amplitude and t_0 is the onset time.

For statistical analysis, normality of data distribution was assessed using the Shapiro–Wilk test, and homogeneity of variances using Levene's test. Based on these results, the Mann–Whitney U test was used to compare between species. Effect sizes were calculated using Cohen's *d*. Data are presented as mean ± standard error of the mean (SEM), and statistical significance was set at $p < 0.05$.

To further examine the temporal dynamics of large and small turns during pulse stimuli, turn angle distributions were generated in 100 ms bins for Figure 4 (and in 200 ms bins for Figure 5), and fitted using a mixture of three Gaussian distributions:

$$P(\theta) = \frac{A_{\text{left}} e^{-\frac{(\theta-\mu_{\text{left}})^2}{2\sigma_{\text{left}}^2}} + A_{\text{right}} e^{-\frac{(\theta-\mu_{\text{right}})^2}{2\sigma_{\text{right}}^2}} + A_{\text{small}} e^{-\frac{(\theta-\mu_{\text{small}})^2}{2\sigma_{\text{small}}^2}}}{A_{\text{left}} + A_{\text{right}} + A_{\text{small}}}$$

As turn characteristics differ by species, we used the following parameters for fitting: Zebrafish: μ_{right}= -40.0, μ_{left}= 40.0, σ_{right}= 20.0, σ_{left}= 20.0, σ_{smal}= 6.0; Medaka: μ_{right}= -45.0, μ_{left}= 45.0, σ_{right}= 20.0, σ_{left}= 20.0, σ_{smal}= 15.0. From the fits, we extracted the amplitude of large turns (Amp_{left}, Amp_{right}) and the directional bias of small turns (μ_{small}). The temporal dynamics of these parameters were then analyzed by fitting exponential curves to estimate time constants.

Alternative stimuli and frequency domain analysis

Sinusoidal motion stimuli were generated with dot velocities modulated according to $v(t) = v_0 \times \sin(2\pi ft)$, where v_0 = 10 mm/s maximum velocity amplitude and f was the stimulus frequency (positive: leftward, negative: rightward). Stimulus frequencies were tested at (1/0.1)*2π, (1/0.2)*2π, (1/0.3)*2π, (1/0.5)*2π, (1/0.7)*2π, and 2π Hz. Each frequency condition was presented for 20 seconds after 5 seconds of open-loop converging stimuli. Stimulus order was randomized across trials. Turning angles were calculated as described in the "Behavioral Analysis" section. For each frequency condition, mean turning angles were computed across all individuals within a 200ms time bin. Then time series of average turning angles were fitted with the function $\theta(t) = A \times \sin(2\pi ft + \varphi) + \theta_0$ using least-squares optimization (scipy.optimize.curve_fit). Response amplitude (A) and phase lag (φ) were extracted for each frequency condition. To analyze the temporal dynamics of big turns and small turns, for each 200 ms time bin, individual fish turn angle distributions were generated and fitted with three-component Gaussian mixture models as described in the "Estimation of time constants" section. This yielded temporal traces of: big turn proportion (L- R) and Bias of small turn. Temporal dynamics of big turn proportions and small turn bias were fitted with sinusoidal functions using the same procedure as for average turning angles. Component-specific amplitude and phase responses were extracted to characterize frequency dependencies of underlying control systems.

Modeling and simulation

To simulate the temporal dynamics of optomotor responses to whole-field motion, we developed a mechanistic model based on hypothesized neural control circuits in fish larvae. The model incorporates two independent control systems: (1) proportional control, governing big turn probabilities and (2) bias control, governing small turn direction.

Each control system implements first-order dynamics with two key parameters: input gain (g_0) determining sensitivity to visual stimuli, and decay rate (g_1) controlling the temporal persistence of neural activity. The temporal evolution of neural responses was computed using the Euler method with time step dt = 0.01 s:

$$\frac{dL}{dt} = g_{\text{prop},0} \times \text{stimulus}_{\text{left}} - g_{\text{prop},1} \times L$$

$$\frac{dR}{dt} = g_{\text{prop},0} \times \text{stimulus}_{\text{right}} - g_{\text{prop},1} \times R$$

$$\frac{dS}{dt} = g_{\text{bias},0} \times \text{stimulus}_{\text{difference}} - g_{\text{bias},1} \times S$$

where R and L represent right and left big turn activities, and F represents small turn bias. Visual stimuli were processed asymmetrically: for leftward motion, *stimulus_left* = 1.0 and *stimulus_right* = -0.1; for rightward motion, these values were reversed.

In addition, we implemented transport delays (100 ms) for big turns in both species, which could arise from neural transport delays, second-order membrane dynamics, or a combination of both mechanisms.

Then, neural activities were converted to behavioral outputs through a three-component Gaussian mixture model as described in the “Estimation of time constants” section. Also, as a realistic model, we estimated that both left, right, and small turns control have a baseline activity. A saturation boundary was applied to prevent unrealistic neural activities, described as the “softmax” parameter in Figure 6.

Parameter Fitting and Validation

Model parameters were fitted to experimental results of unidirectional stimuli using the component-based approach: we directly fitted the left-right difference (LRs = L - R) and small turn bias (S) components, allowing average turning angles to emerge naturally from the angle distribution function. This mechanistically sound approach ensures that fitted components correspond to hypothesized neural pathways.

Non-linear least squares optimization (scipy.optimize.minimize of python package) was used with the L-BFGS-B algorithm and multiple random initial conditions to avoid local minima. Fitting quality was assessed using the coefficient of determination (R^2): $R^2 = 1 - (SS_res / SS_tot)$ where SS_res is the sum of squared residuals and SS_tot is the total sum of squares. Separate R^2 values were calculated for fitted components (LRs, F) and emergent average angles.

To validate model predictions across different stimulus conditions, we tested the fitted parameters against alternating sinusoidal motion stimuli at frequencies ranging from 0.1 to 10 Hz. Model responses were analyzed in the frequency domain using Fourier analysis to extract amplitude and phase characteristics, enabling comparison with experimental frequency response data.

Statistics

(Figure 2d,e) Turn angle data were analyzed using a two-way mixed analysis of variance (ANOVA) with visual stimuli (whole-rig stimuli vs. restricted stimuli) as a between-subjects factor and spatial bin (bins ‘0-‘ – ‘50-‘, from wall to center) as a within-subjects factor. Average turning angles calculated for each fish in each spatial bin. Following significant main effects or interactions, post-hoc analyses were conducted. For the main effect of spatial bin, pairwise comparisons with Bonferroni correction were performed to determine differences in turning angles between spatial locations. For the significant stimuli × spatial bin interaction, simple main effect analyses were conducted by comparing stimuli differences at each spatial bin using independent samples t-tests with Bonferroni correction for multiple comparisons. Effect sizes were reported as partial eta-squared (ηp^2) for ANOVA effects and Cohen's d for pairwise comparisons. Statistical significance was set at $p < 0.05$. All statistical analyses were performed using Python (version 3.10.13) with the pingouin (version 0.5.5) and scipy (version 1.10.1) packages.

(Figure 2j) Statistical analyses were performed using Python (version 3.10.13) with SciPy (version 1.10.1) and NumPy (version 3.10) libraries. Data are presented as mean ± standard deviation (STD). Sample sizes were n=10 for zebrafish and n=12 for medaka. The normality of data distribution in each group was assessed using the Shapiro-Wilk test. As both groups showed normal distribution (Shapiro-Wilk test, $p > 0.05$, zebrafish: 0.5894, medaka: 0.2263), statistical comparisons between groups were performed using Welch's t-test, which does not assume equal variances between groups.

(Figure 2n) The cancel effect size was quantified as the zero-crossing point of the interpolated function of the inside-disk angle and turn angle. To compare the cancel effect size between zebrafish (n=6) and medaka (n=10), we calculated the average effect across 15 trials for each individual fish. The normality of data distribution was assessed using Shapiro-Wilk tests, and homogeneity of variances was evaluated using Levene's test. Based on these results, Student's t-test was used to

compare between species. Effect size was calculated as Cohen's d. Data are presented as the mean ± standard error of the mean (SEM). Statistical significance was set at $p < 0.05$. All statistical analyses were performed using Python Python (version 3.10.13), with scipy (version 1.10.1), statsmodels (version 0.14.0), and (version 0.5.5) packages.

(*Figure 3*) To compare the ability to respond to short lifetime of dots between zebrafish (n=7) and medaka (n=12), we calculated the average of the time constants across 20 trials for each individual fish. The normality of data distribution was assessed using Shapiro-Wilk tests, and homogeneity of variances was evaluated using Levene's test. Based on these results, Welch's t-test was used to compare between species. Statistical significance was set at $p < 0.05$.

(***Figure 4***) Confidence intervals for fitted sine wave parameters were calculated using the covariance matrix obtained from the nonlinear least-squares fitting procedure. Parameter standard errors were derived as the square root of the diagonal elements of the covariance matrix. Confidence intervals were then computed using the t-distribution with degrees of freedom equal to the number of data points minus the number of fitted parameters (n - 3). The confidence interval half-width for each parameter was calculated as the product of the critical t-value ($\alpha = 0.05$ for 95% confidence intervals) and the corresponding parameter standard error. For phase measurements, confidence intervals exceeding 360° were capped at this maximum value to reflect the periodic nature of the parameter. Fitting quality was assessed using the coefficient of determination (R^2) and reduced chi-squared statistics, with the latter calculated as the sum of squared residuals divided by the degrees of freedom.

Data access

Behavioral data is submitted to Dryad (DOI: 10.5061/dryad.gxd2547wg). Code for analysis is shared in the github link (https://github.com/yasukoisoe/cross_species_OMR).

Contributions

Conceptualization, YI, and FE; Methodology, YI, FE; Data analysis, YI; Statistics, YI, YM, MB; Writing - Original Draft, YI; Writing - Review & Editing, YI, and FE; Visualization, YI, YM; Funding Acquisition, FE.

Acknowledgement

We are grateful to the Engert lab and the Fishman lab at Harvard University for experimental and conceptual support. We thank Dr. Roy Harpaz at Harvard University for critical discussion. We thank Dr. Armin Bahl at Konstanz Institute for experimental support and thoughtful suggestions in behavioral rigs and analysis. Florian Engert received funding from the National Institutes of Health (U19NS104653 and 1R01NS124017-01), DoD (W911NF2420112) and the Simons Foundation (SCGB 542973 and NC-GB-CULM-00003241-02). Yasuko Isoe acknowledges the Uehara Memorial Foundation and Japan Society for Promoting Science for fellowship funding.

Competing interests

The authors declare no competing interests.

Reference

Alexander, Emma, Lanya T. Cai, Sabrina Fuchs, Tim C. Hladnik, Yue Zhang, Venkatesh Subramanian, Nicholas C. Guilbeault, et al. 2022. “Optic Flow in the Natural Habitats of Zebrafish Supports Spatial Biases in Visual Self-Motion Estimation.” *Current Biology : CB* 32 (23): 5008–21.e8.

Baden, Tom, Timm Schubert, Le Chang, Tao Wei, Mariana Zaichuk, Bernd Wissinger, and Thomas Euler. 2013. “A Tale of Two Retinal Domains: Near-Optimal Sampling of Achromatic Contrasts in Natural Scenes through Asymmetric Photoreceptor Distribution.” *Neuron* 80 (5): 1206–17.

Bahl, Armin, and Florian Engert. 2020. “Neural Circuits for Evidence Accumulation and Decision Making in Larval Zebrafish.” *Nature Neuroscience* 23 (1): 94–102.

Borst, Alexander, Juergen Haag, and Dierk F. Reiff. 2010. “Fly Motion Vision.” *Annual Review of Neuroscience* 33:49–70.

Carbo-Tano, Martin, Mathilde Lapoix, Xinyu Jia, Olivier Thouvenin, Marco Pascucci, François Auclair, Feng B. Quan, et al. 2023. “The Mesencephalic Locomotor Region Recruits V2a Reticulospinal Neurons to Drive Forward Locomotion in Larval Zebrafish.” *Nature Neuroscience* 26 (10): 1775–90.

Chen, Alex B., Diptodip Deb, Armin Bahl, and Florian Engert. 2021. “Algorithms Underlying Flexible Phototaxis in Larval Zebrafish.” *The Journal of Experimental Biology* 224 (10). https://doi.org/10.1242/jeb.238386.

Clark, David Thomas. 1981. *Visual Responses in Developing Zebrafish (Brachydanio Rerio)*.

Dusenbery, David B. 1992. *Sensory Ecology: How Organisms Acquire and Respond to Information*. W H Freeman & Company.

Engeszer, Raymond E., Larissa B. Patterson, Andrew A. Rao, and David M. Parichy. 2007. “Zebrafish in the Wild: A Review of Natural History and New Notes from the Field.” *Zebrafish* 4 (1): 21–40.

Furutani-Seiki, Makoto, and Joachim Wittbrodt. 2004. “Medaka and Zebrafish, an Evolutionary Twin Study.” *Mechanisms of Development* 121 (7-8): 629–37.

Groschner, Lukas N., Laura Chan Wah Hak, Rafal Bogacz, Shamik DasGupta, and Gero Miesenböck. 2018. “Dendritic Integration of Sensory Evidence in Perceptual Decision-Making.” *Cell* 173 (4): 894–905.e13.

Harada, Yumi, Megumi Matsuo, Yasuhiro Kamei, Mayuko Goto, and Shoji Fukamachi. 2019. “Evolutionary History of the Medaka Long-Wavelength Sensitive Genes and Effects of Artificial Regression by Gene Loss on Behavioural Photosensitivity.” *Scientific Reports* 9 (1): 2726.

Harpaz, Roy, Minh Nguyet Nguyen, Armin Bahl, and Florian Engert. 2021. “Precise Visuomotor Transformations Underlying Collective Behavior in Larval Zebrafish.” *Nature Communications* 12 (1): 6578.

Hilgers, Leon, and Julia Schwarzer. 2019. “The Untapped Potential of Medaka and Its Wild Relatives.” *eLife* 8 (July). https://doi.org/10.7554/eLife.46994.

Imada, Haruka, Masahito Hoki, Yuji Suehiro, Teruhiro Okuyama, Daisuke Kurabayashi, Atsuko Shimada, Kiyoshi Naruse, Hiroyuki Takeda, Takeo Kubo, and Hideaki Takeuchi. 2010. “Coordinated and Cohesive Movement of Two Small Conspecific Fish Induced by Eliciting a Simultaneous Optomotor Response.” *PloS One* 5 (6): e11248.

Isoe, Yasuko, Yumi Konagaya, Saori Yokoi, Takeo Kubo, and Hideaki Takeuchi. 2016. “Ontogeny and Sexual Differences in Swimming Proximity to Conspecifics in Response to Visual Cues in Medaka Fish.” *Zoological Science* 33 (3): 246–54.

Lee, Joseph J., et al. “MORE POWERFUL MULTIPLE TESTING IN RANDOMIZED EXPERIMENTS WITH NON-COMPLIANCE.” *Statistica Sinica*, vol. 27, no. 3, 2017, pp. 1319–45. *JSTOR*, http://www.jstor.org/stable/26383257.

Leem, Joo-Baek, Wonju Jeon, Chi-Young Yun, and Sang-Hee Lee. 2012. “Quantitative Analysis of Fish Schooling Behavior with Different Numbers of Medaka (Oryzias Latipes) and Goldfish (Carassius Auratus).” *Ocean Science Journal: OSJ* 47 (4): 445–51.

Lucon-Xiccato, Tyrone, Francesca Conti, Felix Loosli, Nicholas S. Foulkes, and Cristiano Bertolucci. 2020. “Development of Open-Field Behaviour in the Medaka,.” *Biology* 9 (11). https://doi.org/10.3390/biology9110389.

Marshall, Justin. 2017. “Vision and Lack of Vision in the Ocean.” *Current Biology : CB* 27 (11): R494–502.

Massey, Frank J. “The Kolmogorov-Smirnov Test for Goodness of Fit.” *Journal of the American Statistical Association*, vol. 46, no. 253, 1951, pp. 68–78. *JSTOR*, https://doi.org/10.2307/2280095.

Michael, Sabrina C. J., Jon Patman, and Marvin M. F. Lutnesky. 2021. “Water Clarity Affects Collective Behavior in Two Cyprinid Fishes.” *Behavioral Ecology and Sociobiology* 75 (8). https://doi.org/10.1007/s00265-021-03060-x.

Murata, K., M. Kinoshita, K. Naruse, M. Tanaka, and Kamei Y. (Eds.). 2019. “Medaka: Biology, Management, and Experimental Protocols, Volume 2.” https://books.google.com/books?hl=en&lr=&id=PbKrDwAAQBAJ&oi=fnd&pg=PA15&dq=medaka+eggs+sticky+hairs+around+the+chorions,+and+medaka+mothers+carry+and+glue+eggs+onto+the+root+of+water+grasses+after+breeding&ots=R3HQ2u4zde&sig=Z9MmXwO24ygHjLX1ET7EFvXuy_c.

Nasiadka, Andrzej, and Matthew D. Clark. 2012. “Zebrafish Breeding in the Laboratory Environment.” *ILAR Journal* 53 (2): 161–68.

Naumann, Eva A., James E. Fitzgerald, Timothy W. Dunn, Jason Rihel, Haim Sompolinsky, and Florian Engert. 2016. “From Whole-Brain Data to Functional Circuit Models: The Zebrafish Optomotor Response.” *Cell* 167 (4): 947–60.e20.

Neyman, J. “Fiducial Argument and the Theory of Confidence Intervals.” *Biometrika*, vol. 32, no. 2, 1941, pp. 128–50. *JSTOR*, https://doi.org/10.2307/2332207. Accessed 29 July 2023.

Ochiai, Takashi, Yuji Suehiro, Katsuhiro Nishinari, Takeo Kubo, and Hideaki Takeuchi. 2013. “A New Data-Mining Method to Search for Behavioral Properties That Induce Alignment and Their Involvement in Social Learning in Medaka Fish (Oryzias Latipes).” *PloS One* 8 (9): e71685.

Olveczky, Bence P., Stephen A. Baccus, and Markus Meister. 2003. “Segregation of Object and Background Motion in the Retina.” *Nature* 423 (6938): 401–8.

Oteiza, Pablo, and Maude W. Baldwin. 2021. “Evolution of Sensory Systems.” *Current Opinion in Neurobiology* 71 (December):52–59.

Rajan, Gokul, Julie Lafaye, Giulia Faini, Martin Carbo-Tano, Karine Duroure, Dimitrii Tanese, Thomas Panier, et al. 2022. “Evolutionary Divergence of Locomotion in Two Related Vertebrate Species.” *Cell Reports* 38 (13): 110585.

Rubin, Donald B. “Randomization Analysis of Experimental Data: The Fisher Randomization Test Comment.” *Journal of the American Statistical Association*, vol. 75, no. 371, 1980, pp. 591–93. *JSTOR*, https://doi.org/10.2307/2287653.

Sato, Keita, Takahiro Yamashita, Yoshihiro Haruki, Hideyo Ohuchi, Masato Kinoshita, and Yoshinori Shichida. 2016. “Two UV-Sensitive Photoreceptor Proteins, Opn5m and Opn5m2 in Ray-Finned Fish with Distinct Molecular Properties and Broad Distribution in the Retina and Brain.” *PloS One* 11 (5): e0155339.

Spence, R., M. K. Fatema, M. Reichard, K. A. Huq, M. A. Wahab, Z. F. Ahmed, and C. Smith. 2006. “The Distribution and Habitat Preferences of the Zebrafish in Bangladesh.” *Journal of Fish Biology* 69 (5): 1435–48.

Suzuki, Risa, Jia Zheng Woo, Thomas Thumberger, Gero Hofmann, Joachim Wittbrodt, and Tinatini Tavhelidse-Suck. 2024. “Characterizing Medaka Visual Features Using a High-Throughput Optomotor Response Assay.” *PloS One* 19 (6): e0302092.

Thiele, Tod R., Joseph C. Donovan, and Herwig Baier. 2014. “Descending Control of Swim Posture by a Midbrain Nucleus in Zebrafish.” *Neuron* 83 (3): 679–91.

Tohya, Shusaku, Atsushi Mochizuki, and Yoh Iwasa. 2003. “Difference in the Retinal Cone Mosaic Pattern between Zebrafish and Medaka: Cell-Rearrangement Model.” *Journal of Theoretical*

Biology 221 (2): 289–300.
Wang, Kun, Julian Hinz, Yue Zhang, Tod R. Thiele, and Aristides B. Arrenberg. 2020. “Parallel Channels for Motion Feature Extraction in the Pretectum and Tectum of Larval Zebrafish.” *Cell Reports* 30 (2): 442–53.e6.
Wei, Wei, Aaron M. Hamby, Kaili Zhou, and Marla B. Feller. 2011. “Development of Asymmetric Inhibition Underlying Direction Selectivity in the Retina.” *Nature* 469 (7330): 402–6.
Widrick, Jeffrey J., Matthias R. Lambert, Louis M. Kunkel, and Alan H. Beggs. 2023. “Optimizing Assays of Zebrafish Larvae Swimming Performance for Drug Discovery.” *Expert Opinion on Drug Discovery* 18 (6): 629–41.
Yoshimatsu, Takeshi, Cornelius Schröder, Noora E. Nevala, Philipp Berens, and Tom Baden. 2020. “Fovea-like Photoreceptor Specializations Underlie Single UV Cone Driven Prey-Capture Behavior in Zebrafish.” *Neuron* 107 (2): 320–37.e6.
Zabrocki, L., Leroutier, M., & Bind, M. (2021, April 19). Estimating the Local Air Pollution Impacts of Maritime Traffic: A Principled Approach for Observational Data. https://doi.org/10.31219/osf.io/v7ctk
Zimmermann, Maxime J. Y., Noora E. Nevala, Takeshi Yoshimatsu, Daniel Osorio, Dan-Eric Nilsson, Philipp Berens, and Tom Baden. 2018. “Zebrafish Differentially Process Color across Visual Space to Match Natural Scenes.” *Current Biology : CB* 28 (13): 2018–32.e5.